Phase change in $CoTi_2$ induced by MeV electron irradiation

Akihiro Zensho[a], Kazuhisa Sato[a,b,*], Hidehiro Yasuda[a,b], and Hirotaro Mori[b]

[a]Division of Materials and Manufacturing Science, Graduate School of Engineering, Osaka University, 2-1 Yamada-Oka, Suita, Osaka 565-0871, Japan
[b]Research Centre for Ultra-High Voltage Electron Microscopy, Osaka University, 7-1 Mihogaoka, Ibaraki, Osaka 567-0047, Japan

*Corresponding author: Tel.: +81-6-6879-7941; fax: +81-6-6879-7942; e-mail: sato@uhvem.osaka-u.ac.jp

Abstract

The phase change induced by MeV electron irradiation in the intermetallic compound $E9_3$-$CoTi_2$ was investigated using high-voltage electron microscopy. Under MeV electron irradiation, $CoTi_2$ was first transformed into an amorphous phase and, with continued irradiation, crystallite formation in the amorphous phase (i.e. formation of crystallites of a solid-solution phase within the amorphous phase) was induced. The critical temperature for amorphisation was around 250 K. The total dose (dpa) required for crystallite formation (i.e. that required for partial crystallisation) remained high (i.e. 27–80 dpa) and, even after such high doses, the amorphous phase was retained in the irradiated sample. Such partial crystallisation behaviour of amorphous $Co_{33}Ti_{67}$ was clearly different from the crystallisation behaviour (i.e. amorphous-to-solid solution, polymorphous transformation) of amorphous $Cr_{67}Ti_{33}$ reported in the literature. A possible cause of the difference is discussed.

Keywords:

· Electron irradiation
· Partial crystallisation
· In situ electron microscopy
· High-voltage electron microscopy
· Intermetallic compounds

1. Introduction

A solid-state phase transition from an equilibrium crystalline phase (hereafter denoted by C^e) to a non-equilibrium crystalline phase (hereafter denoted by C^n) is one of the most important topics in both fundamental and applied materials science. Such a phase transition can be successfully achieved by agitation with stimuli such as mechanical grinding (MG), ion irradiation, and electron irradiation. Details of the individual phase transitions induced by these stimuli can be found in various publications [1-4].

Of these stimuli, electron irradiation, especially in situ MeV electron irradiation with a high-voltage

electron microscope (HVEM), has been attracting attention because it has the following advantages over the others: (i) contamination of samples can be suppressed to a low level, unlike the case with MG; (ii) cascades in which complex atomic processes might be operating [5] are absent, as opposed to the case with ion irradiation; and (iii) the phase transition can be directly observed using electron microscopy techniques simultaneously with the introduction of atom displacements (i.e. atomic defects).

Recently, HVEM observations which will improve our understanding of the phase transition from C^e to C^n have been reported [6,7]. These results suggest that the phase transition can occur by one of two main routes. One is a route via an amorphous state, observed in Cr_2Ti [6], and in this case the Gibbs free energy of the alloy first increases upon amorphisation (i.e. amorphisation of C^e) and then decreases upon crystallisation (i.e. crystallisation to C^n). In the other route, C^e is transformed directly into C^n, as observed in σ-CrFe [7], without any intermediate amorphous state; in this case the Gibbs free energy of the alloy is considered to increase monotonically (see note 1 for an explanation of the use of the word 'monotonically') during the phase transition. The former observation regarding Cr_2Ti is in line with the original observation by Sinkler et al. [8].

The above phase transition observed in Cr_2Ti is unique in that only a few dpa were enough to induce crystallisation of an amorphous phase to a C^n [i.e. a body-centred cubic (bcc) solid solution] [6], and upon crystallisation, grain growth of the C^n occurred on such an extensive scale that the C^n replaced the whole amorphous phase within an irradiated volume [6,8]. The transition from the C^e to the C^n via an amorphous phase can therefore be regarded as a polymorphous transition which involves no change in composition. In this paper, such a crystalline-to-amorphous-to-crystalline transition is referred to simply as a C^e–A–C^n transition, and intermetallic compounds which show such a C^e–A–C^n transition are referred to as category I intermetallic compounds, which can be rendered amorphous by MeV electron irradiation. (To the authors' knowledge, only Cr_2Ti is known to belong to this category.)

After the original observation of the C^e–A–C^n transition in Cr_2Ti by Sinkler et al. [8], observations of a phase change in which a C^e was first rendered amorphous by MeV electron irradiation and then on continued irradiation crystallites (tiny crystalline grains) appeared within the amorphous phase, have been reported for some intermetallic compounds (see review paper [9]). Features of the crystallite formation are as follows. A large total dose (larger than a few tens of dpa) was needed and crystallisation was not complete, therefore a certain amount of amorphous phase always remained. In the present paper, intermetallic compounds showing such a phase change under MeV electron irradiation are referred to as category II intermetallic compounds, which can be rendered amorphous by MeV electron irradiation.

The aim of the present work is to investigate the response of the intermetallic compound $CoTi_2$ with the $E9_3$ structure to MeV electron irradiation by using the in situ HVEM technique, and to clarify whether this compound is category I, category II, or neither. The results show that $CoTi_2$ falls in category II. A brief discussion of a possible cause, which would enable distinction between categories I and II, is presented.

2. Experimental procedures

Master ingots of $Co_{33}Ti_{67}$ alloy were prepared by arc-melting high-purity cobalt (99.93 mass%) and titanium (99.9 mass%) in a highly purified Ar atmosphere. The ingots were sliced into plates of thickness about 500 μm using a diamond wheel saw. Thin films for transmission electron microscopy (TEM) and MeV electron irradiation were prepared by ion thinning using Ar ions. The accelerating voltage and ion incident angle were maintained at 4.5 kV and 4°, respectively. The damaged layer possibly formed during ion thinning was removed using Ar ion beams of energy below 2 keV.

Microstructural observations and MeV electron irradiation of foil samples were performed at Osaka University using HVEM (Hitachi H-3000) at an accelerating voltage of 2 MV. The main phase in the samples was $E9_3$-$CoTi_2$ (the phase diagram of the Co–Ti binary system is available in the literature [10]). The electron irradiation temperature and electron dose rate were 103–290 K and 6.7×10^{24} m^{-2} s^{-1} to 7.3×10^{24} m^{-2} s^{-1}, respectively. The changes in the microstructure during electron irradiation were examined using in situ TEM with HVEM, to capture bright-field (BF) images and selected area electron diffraction (SAED) patterns. The size of the SA aperture was, in most cases, 5 μmφ, corresponding to 170 nmφ on the image plane. In addition, for some post-irradiated specimens, the microstructures were also studied using a 200 kV scanning transmission electron microscope (STEM; JEOL ARM200F) to obtain atomic-scale information on the structure.

As previously reported [11], the cross sections of atomic displacement in pure Co and Ti are estimated to be 66 barns for 2.0 MeV electron, based on the McKinley–Feshbach formula [12, 13]. However, there are no reliable methods for quantitatively evaluating the atomic displacement of the constituent elements in compounds [11]. In the present study, it is therefore assumed that a cross section for atomic displacement of 66 barns also holds for $E9_3$-$CoTi_2$. Using this value, the damage rates were estimated to range from 4.4×10^{-2} dpa s^{-1} to 4.8×10^{-2} dpa s^{-1}.

3. Results

3.1. Response to MeV electron irradiation as function of temperature

The electron-irradiation-induced phase change of $E9_3$-$CoTi_2$ was studied in situ using HVEM over the temperature range 103–250 K.

Figure 1 shows an example of the results obtained at 140 K; Figure 1(a) to (f) are sequential BF images of a fixed area, Figure 1(a') to (f') show the corresponding SAED patterns, and Figure 1(e'') and (f'') are magnified BF images corresponding to Figure 1(e) and (f), respectively. The BF image before irradiation shows crystalline contrast (e.g. distinct bend contours) (Figure 1a), and the corresponding SAED pattern can be consistently indexed to the [110] net pattern of a crystal with the $E9_3$ structure (Figure 1a'). After irradiation for 10 s, a region of featureless contrast appeared in the central area of electron irradiation (Figure 1b), and only halo rings were seen in the SAED pattern taken from the region (Figure 1b'). This indicates that the equilibrium $E9_3$-$CoTi_2$ phase was rendered amorphous and an amorphous single phase was formed under electron irradiation. With continued irradiation, the amorphous region grew in size, as seen from Figure 1(c) and (d). After irradiation for 1.2×10^3 s, 10

nm-scale fine crystallites appeared near the centre of the amorphous region (i.e. near the central area of electron irradiation), as seen from the magnified BF image shown in Figure 1(e''). At the same time, segmented Debye–Scherrer rings superimposed on the original halo pattern appeared (Figure 1e'). After irradiation for 1.8×10^3 s, the size and number density of crystallites, and the intensity of the Debye–Scherrer rings from the crystallites, increased, as seen from Figure 1(f'') and (f'). This indicates that crystallite formation in the amorphous phase (i.e. partial crystallisation of the amorphous phase) was induced by prolonged electron irradiation. The Debye–Scherrer rings in Figure 1(f'), which are superimposed on halos from the retained amorphous phase, can be consistently indexed to polycrystalline rings from a crystal with the hexagonal close-packed (hcp) structure. No superlattice reflections were observed in the SAED pattern, therefore the crystallites in Figure 1(f'') are considered to be of a solid solution with the hcp structure. [Figure 1 should be placed around here.]

Figure 2 shows an example of the results obtained at 220 K; sequential BF images and the corresponding SAED patterns are shown in Figure 2(a) to (f) and Figure 2(a') to (f'), respectively. Magnified BF images corresponding to Figure 2(d) to (f) are shown in Figure 2(d'') to (f''), respectively. The BF images before irradiation show a number of distinct bend contours (Figure 2a), and the corresponding SAED pattern can again be consistently indexed to the [110] net pattern of a crystal with the $E9_3$ structure (Figure 2a'). Electron irradiation at 220 K induced phase changes essentially similar to those at 140 K. However, based on a comparison of Figure 2 with Figure 1, the following difference should be noted; the irradiation period required for amorphisation increased from 10 s at 140 K (Figure 1b and b') to 60 s at 220 K (Figure 2c and c'), whereas the period required for crystallite formation in the amorphous phase decreased from 1.2×10^3 s at 140 K (Figure 1e' and e'') to 600 s at 220 K (Figure 2d' and d'') at a fixed electron dose rate of 6.7×10^{24} m^{-2} s^{-1}. The Debye–Scherrer rings in Figure 2(f') can be indexed to polycrystalline rings from the same solid solution crystal as that observed in Figure 1(f') and (f''). [Figure 2 should be placed around here.]

It should be noted that amorphisation took place after irradiation for 180 s at 240 K and after irradiation for 1.2×10^3 s at 250 K.

3.2. Crystallite formation by irradiation at 290 K

As shown in Figures 1 and 2, with prolonged irradiation, crystallite formation in the amorphous phase (i.e. partial crystallisation of the amorphous phase) was induced. The crystallites formed were investigated in detail as follows. An amorphous phase was first produced at a low temperature and then subjected to irradiation at a higher temperature, at which grain growth was expected to occur on a large scale.

Figure 3 gives an example of the results, and shows a series of BF images with the corresponding SAED patterns. The figure shows a crystalline ($E9_3$-$CoTi_2$)-to-amorphous transition induced by irradiation at 103 K (Figure 3a and a', and Figure 3b and b') and subsequent crystallite formation in the amorphous phase (i.e. partial crystallisation of the amorphous phase) induced by irradiation at 290 K (Figure 3c and c' to Figure 3f and f'). Figure 3(d''), (e''), and (f'') are magnified BF images corresponding to Figure 3(d), (e), and (f), respectively. Figure 3(b) shows that an amorphous region of size

approximately 1 μm was produced near the centre of the field by irradiation at 103 K. After irradiation for 180 s at 290 K, fine 10 nm-scale crystallites appeared in the amorphous region, as seen in Figure 3(d''), and segmented Debye–Scherrer rings, albeit of weak intensity, superimposed on the halo pattern appeared, as seen in Figure 3(d'). The size and number density of crystallites, and the intensities of the Debye–Scherrer rings from the crystallites, increased with increasing electron dose, as seen from Figure 3(e') and (e''), and Figure 3(f') and (f''). This indicates that partial crystallisation of the amorphous phase (i.e. the amorphous $Co_{33}Ti_{67}$ alloy) was induced to a large extent by irradiation at a high temperature, i.e. 290 K. A detailed analysis of the Debye–Scherrer rings in Figure 3(f') indicates that the rings can be consistently indexed to polycrystalline rings from the same solid solution crystal as that observed in Figure 1(f') and (f''), i.e. the crystallites are considered to be a solid solution with the hcp structure embedded in the retained amorphous phase, the residual halos from which are clearly seen in Figure 3(f'). [Figure 3 should be placed around here.]

Next, STEM analyses of the crystallites were conducted. Figure 4(a) shows a BF STEM image of crystallites formed by irradiation at 290 K for 3.6×10^3 s (the specimen is the same as that shown in Figure 3f''). In Figure 4(b), which is an enlarged image of the area marked by a square in Figure 4(a), 0.23 nm lattice fringes can be clearly seen. The fast Fourier transformation (FFT) pattern (Figure 4c) taken from the area can be consistently indexed to the FFT pattern from a lattice image of a hcp crystal with lattice constants a = 0.29 nm and c = 0.45 nm. Again, superlattice reflections are absent. In short, it can therefore be said that under MeV electron irradiation $E9_3$-$CoTi_2$ first undergoes a crystalline-to-amorphous transition at lower temperatures (e.g. at 103 K), followed by subsequent partial crystallisation at higher temperatures (e.g. at 290 K), and that the crystallites formed can be regarded as a solid-solution phase with the hcp structure embedded in the retained amorphous phase. [Figure 4 should be placed around here.]

3.3. Total doses for amorphisation and for crystallite formation plotted against temperature

Figure 5 summarises the temperature dependences of the total doses (dpa) needed for amorphisation (open circles) and for crystallite formation (filled squares) under 2 MeV electron irradiation; open circles indicate the total dose at which the SAED pattern taken from the central area of irradiation changed from a crystalline, net pattern to an amorphous, halo pattern during irradiation, and filled squares indicate the total dose at which fine crystallites of size approximately 10 nm appeared in the magnified BF images of the amorphous phase and segmented Debye–Scherrer rings appeared in the corresponding SAED patterns. [Figure 5 should be placed around here.]

Figure 5 shows that amorphisation occurred easily at lower temperatures but became more difficult with increasing irradiation temperature. This behaviour is consistent with that generally observed in a number of electron-irradiation-induced amorphisations of intermetallic compounds [4, 11, 14]. The critical temperature T_c for amorphisation was determined to be approximately 250 K for the present compound. It is considered that under irradiation at temperatures above the T_c atom diffusion in the compound becomes so vigorous that chemical disordering in the compound is kept at a low enough level [14] for the compound to maintain the original $E9_3$ structure.

In contrast, the filled squares in Figure 5 indicate that the total dose for crystallite formation shows weak (see Note 2 for the reason for use of the word 'weak') negative temperature dependence over the range from 103 to 220 K. With regard to the weak temperature dependence, there is a possibility that under MeV electron irradiation, diffusion in the amorphous $Co_{33}Ti_{67}$ alloy at such low temperatures takes place by a modified displacement–mixing mechanism involving a thermally activated process. (For details of the classical displacement–mixing mechanism with no temperature dependence, refer to, for example, reference [15].) However, details of the process are not clear at present.

Figure 5 also shows a measured point (i.e. a filled square at 290 K) obtained by the 103 K/290 K step experiment shown in Figure 3.

4. Discussion

Under MeV electron irradiation, the present $E9_3$-$CoTi_2$ compound first became amorphous. With continued irradiation, crystallite formation in the amorphous phase (i.e. partial crystallisation of the amorphous phase) was induced over the temperature range from 103 to 220 K, as mentioned in section 3.1. The doses (dpa) which were necessary to induce partial crystallisation at three typical temperatures (i.e. 103, 140, and 220 K) are listed in lines three to five in the second column in Table 1. The table summarises the dose (dpa) required to cause crystallisation of (or crystallite formation in) an amorphous phase produced beforehand by MeV electron irradiation, along with the structure of the crystal (i.e. C^n) formed (the third column), the presence or absence of a retained amorphous phase after crystallisation (the fourth column), and literature references quoted (the fifth column) for transition-metal compounds, including $CoTi_2$. To the best of our knowledge, all the transition-metal compounds which have been reported to show electron-irradiation-induced crystallisation behaviours of the corresponding amorphous phase are included (see note 3). In view of the relatively large doses, i.e. 27–80 dpa, and the presence of distinct halos in the SAED patterns (see, for example, Figure 1f' and 2f'), the $CoTi_2$ investigated here is classified as category II (see the sixth column in Table 1), on the basis of the definition in section 1. [Table 1 should be placed around here.]

The first and second lines in the second column in Table 1 show dose (dpa) data for Cr_2Ti at 22 and 103 K, respectively [6,17]. As already described in section 1, crystallisation of amorphous $Cr_{67}Ti_{33}$ occurred at a low dose (i.e. a few dpa), and because no retained amorphous phase was observed after crystallisation, the crystallisation can be regarded as polymorphous. According to the definition, Cr_2Ti is therefore classified as category I (see the sixth column in Table 1).

The dose (dpa) data for Zr_2Cu [18] are shown in the sixth line in the second column in Table 1. In this case, the dose required for crystallite formation (i.e. 120 dpa) was estimated from the electron dose pertaining to Figure 4(c) in reference [18], which apparently corresponds to a state well after the initiation of crystallite formation. This could lead to overestimated values compared with those obtained for $CoTi_2$ in this work, but even after subtraction of the possible overestimate, the appropriate dose is still high, at least a few tens of dpa (i.e. the value in square brackets), because the dose required for amorphisation estimated from the electron dose pertaining to Figure 4(e) in reference [18] was already around 20 dpa. Furthermore, clear halo rings were present in the SAED pattern even after crystallite

formation, as seen in Figure 4(f) in reference [18], indicating the presence of a retained amorphous phase. These facts suggest that amorphous $Zr_{66.7}Cu_{33.3}$ showed only partial crystallisation under MeV electron irradiation.

The dose (dpa) data for Zr_2Pd [9] are shown in the seventh line in the second column in Table 1. In this case, the dose required for crystallite formation (i.e. 214 dpa) was estimated from the electron dose pertaining to Figure 3(c) in reference [9]. After applying a similar correction to that used for Zr_2Cu, the appropriate dose is again considered to be high, at least a few tens of dpa (i.e. the value in square brackets). This is because the dose required for amorphisation estimated from the electron dose pertaining to Figure 3(b) in reference [9] was already around 25 dpa. Furthermore, amorphous halos were again clearly recognised in the SAED pattern even after crystallite formation, as seen in Figure 3(c) in reference [9], indicating the presence of a retained amorphous phase. These facts suggest that amorphous $Zr_{66.7}Pd_{33.3}$ showed only partial crystallisation under MeV electron irradiation.

On the basis of all these facts, it seems reasonable to conclude that both Zr_2Cu and Zr_2Pd can be classified as category II (see the sixth column in Table 1).

We now briefly discuss a possible cause of the distinction between the compounds in category I and II. It has been reported, based on a compilation of literature data, that in thermal crystallisation of amorphous transition-metal alloys, diffusionless polymorphic crystallisation occurs at low temperatures if the formation enthalpy of a simple solid solution (ΔH^{ss}) is lower than that of the amorphous phase (ΔH^{am}) [19]. The crystallisation temperatures are relatively high if ΔH^{ss} is higher than ΔH^{am}, because crystallisation has to occur either by phase separation or into one of the equilibrium compounds [19]. For example, it is possible to estimate from Figure 1 in reference [19] that thermal crystallisation took place at low temperatures, i.e. 220–240 K, when ΔH^{ss} was lower than ΔH^{am} by 6.5 kJ/mol (i.e. −6.5 kJ/mol in terms of $\Delta H^{ss} - \Delta H^{am}$), in amorphous $W_{71}Re_{29}$.

On the basis of this suggestion, information on the difference between the Gibbs free energy of the solid solution (G^{ss}) and that of the amorphous phase (G^{am}) was collected from the literature for the transition-metal compounds listed in Table 1; the data are shown in the seventh column in the table. The values of ($G^{ss} - G^{am}$) for Cr_2Ti (around −6 kJ/mol at both 22 and 103 K) were estimated from Figure 6 in reference [6]. In the case of Zr_2Cu, the value of ($G^{ss} - G^{am}$) (around + 2.5 kJ/mol) was estimated from Figure 2 in reference [20], with the assumption that G^{am} corresponds to the arithmetical mean of the two curves calculated for the amorphous phases (i.e. the curves marked liq. 1 and liq. 2 in the figure) in the alloy system. In addition, in a separate paper on solid-state crystalline–glassy cyclic phase transformations of mechanically alloyed $Cu_{33}Zr_{67}$ powders [21], it was suggested that the formation enthalpy of the metastable bcc phase is comparable to that of the amorphous phase, and that the energy barrier between these two phases is sufficiently low to allow such cyclic transformations [21], i.e. the value of ($G^{ss} - G^{am}$) is small and negative. This information is also included in the seventh column in Table 1. For $CoTi_2$, the value of ($G^{ss} - G^{am}$) (i.e. around −1.7 kJ/mol, note 4) was estimated based on calculations using the thermodynamic data in the literature [22]. This information is included in the seventh column in Table 1.

A comparison of the data in the sixth and seventh columns in Table 1 suggests that it is reasonable

to consider that when the value of ($G^{ss} - G^{am}$) is large and negative, the corresponding compound will fall in category I, whereas if the value is small (i.e. the Gibbs free energy of the solid solution is similar to that of the amorphous phase), the corresponding compound will be category II. This suggests that category I or II can be selected according to the magnitude of the driving force for the amorphous-to-solid solution transition in the absence of irradiation. However, the sample number in Table 1 is small, and it is evident that more work is needed to provide a concrete guide to the cause of the differences between category I and II compounds.

A comprehensive understanding of the phase transition from a C^e to a C^n induced by MeV electron irradiation also requires information on the direct crystalline-to-crystalline (i.e. C^e-to-C^n) transition, in which an amorphous phase does not appear in the intermediate stages of the transition. However, to the best of our knowledge, there are few reports of such direct C^e-to-C^n transitions induced by MeV electron irradiation [7, 23] (see note 5), and the atomistic mechanism behind such a direct crystalline-to-crystalline transition has not yet been clarified. In view of this situation, the following points may be worthy of attention. In a recent theoretical paper [24], it was pointed out that in bcc pure iron a secondary defect with a three-dimensional periodic structure (corresponding to the C15 Laves phase) can be formed by aggregation of primary defects, and it is was reported that such formation of secondary defects can be regarded as a local irradiation-induced phase transformation from bcc to C15 in pure iron. This is of interest because it suggests a possible atomistic mechanism for the direct transition from an equilibrium crystalline phase to a non-equilibrium crystalline phase.

5. Conclusion

The total dose (dpa) required for amorphisation of $CoTi_2$ was low (i.e. below a few dpa) at low temperatures, but increased abruptly at around 250 K, indicating that the critical temperature for amorphisation was around this temperature. In contrast, the total dose (dpa) required for crystallite formation (i.e. for the formation of crystallites of a solid solution) remained high (i.e. 27–80 dpa), and, even after subjection to such high doses, the amorphous phase was retained in the irradiated sample. Such partial crystallisation behaviour of amorphous $Co_{33}Ti_{67}$ is clearly different from the crystallisation behaviour (i.e. amorphous-to-solid solution polymorphous transformation) of amorphous $Cr_{67}Ti_{33}$ reported in literature. It is suggested that the magnitude of the driving force for the amorphous-to-solid solution transformation in the absence of irradiation may responsible for the difference.

Notes

1. The word ‘monotonically’ was used in this paper to emphasise that the transition occurred directly from a C^e with a low Gibbs free energy to a C^n with a higher one. Note that, strictly speaking, in the final stage of the transformation into the C^n, there may be an ‘overshoot’ in the increment in the Gibbs free energy, which would account for the nucleation barrier (i.e. the energy required for the nucleation of C^n in the C^e matrix) to the transformation.

2. The activation energy for the process responsible for the nucleation of crystallites under MeV electron irradiation was estimated as follows. It was first assumed that the total atom flux necessary for nucleation remains constant, irrespective of temperature. Based on this premise, the values of 1/(total dose), measured at 103, 140, and 220 K, were plotted against 1/*T*. The slope of the Arrhenius plot gave 0.01–0.02 eV as the activation energy. This value is low compared to those known for atom migrations, therefore the adjective 'weak' was used here.
3. Quasicrystals were excluded from Table 1.
4. The value was for 298 K.
5. If we confine ourselves to diffusional transformations (except for the displacive transformation), only these two reports on this subject are available in the literature.

Disclosure statement

No potential conflict of interest was reported by the authors.

Funding

This work was supported by the program Collaborative Research Station of High-Voltage Electron Microscopy (FY 2010–FY 2015) of the Ministry of Education, Culture, Sports, Science, and Technology (MEXT), Japan.

Acknowledgment

We thank Helen McPherson, PhD, for editing a draft of this manuscript.

References

[1] H. Bakker, G. F. Zhou and H. Yang, *Mechanically driven disorder and phase transformations in alloys*, Progress in Materials Science 39 (1995), p.p. 159 – 241.

[2] W. L. Johnson, *Thermodynamic and kinetic aspects of the crystal to glass transformation in metallic materials*, Progress in Materials Science 30 (1986), p.p. 81 – 134.

[3] M. Nastasi, J. W. Mayer and J. K. Hirvonen, *Ion-solid interactions : fundamentals and applications*, Cambridge University Press, Cambridge, 1996.

[4] P.R. Okamoto, N.Q. Lam, and L.E. Rehn, *Physics of crystal-to-glass transformations*, in *Solid State Physics*, H. Ehrenreich and F. Spaepen, eds., Academic Press, San Diego, CA, 1999, pp. 65–126.

[5] S. J. Rothman, *Effects of irradiation on diffusion in metals and alloys*, in *Phase transformations during irradiation*, F. V. Nolfi, Jr, ed., Applied Scientific Publishers, London, 1983, p.p. 189–211.

[6] S. Anada, T. Nagase, H. Yasuda and H. Mori, *Electron-irradiation-induced phase transition in Cr_2M (M = Ti and Al) intermetallic compounds*, J. Alloys Compd. 579 (2013), p.p. 646–653.

[7] S. Anada, T. Nagase, K. Kobayashi, H. Yasuda and H. Mori, *Phase stability of σ-CrFe intermetallic compound under fast electron irradiation*, Acta mater. 71(2014), p.p.195-205.

[8] W. Sinkler, D.E. Luzzi, and C.W. Allen, *Electron irradiation of TiM_2 Laves compounds: The influence of β phase stability on amorphization*, Scr. Metall. 28 (1993), p.p. 863–868.

[9] T. Nagase, A. Nino, T. Hosokawa and Y. Umakoshi, *Electron irradiation induced crystal-to-amorphous-to-crystal transition in some metallic glasses*, Materials Transactions 48(2007), p.p. 1651-1658.

[10] J. L. Murray, *Co-Ti phase diagram (1990),* in *Alloy phase Diagrams Database,* P. Villars, H. Okamato, and K. Cenzual, eds., ASM International, Ohio, 2006, p. 900751. Available at http://www1.asminternational.org/asminterprise/apd/default.aspx.

[11] S. Anada, A. Zensho, H. Yasuda and H. Mori, *Phase change of CoTi and Co_3Ti induced by MeV-scale electron irradiation*, Phil. Mag. 96(2016), p.p.2027-2039.

[12] F. Seitz and J.S. Koehler, *Displacement of atoms during radiation*, in *Solid State Physics*, F. Seitz and D. Turnbull, eds., Academic Press, New York, 1956, p.p. 305–448.

[13] J.W. Corbett, *Electron Radiation Damage in Semiconductors and Metals*, Academic Press, New York, 1966.

[14] D.E. Luzzi, H. Mori, H. Fujita, and M. Meshii, *The relationship between the chemical and topological disorder in the intermetallic compound Cu_4Ti_3*, Acta Metall. 34 (1986), pp. 629–639.

[15] H. Wiedersich, *Phase stability and solute segregation during irradiation*, in *Physics of Radiation Effects in Crystals*, R.A. Johnson and A.N. Orlov eds., North-Holland, Amsterdam, 1986, p.p.225-280.

[16] T. Nagase, *Advanced materials design by irradiation of high energy particles*, in *Progress in Advanced Structural and Functional Materials Design*, T. Kakeshita ed., Springer, Tokyo, 2013, p.p.137 – 153.

[17] S. Anada, private communication.

[18] T. Nagase and Y. Umakoshi, *Phase stability of amorphous and crystalline phases in melt-spun $Zr_{66.7}Cu_{33.3}$ alloy under electron irradiation*, Scripta mater. 48 (2003), p.p. 1237 – 1242.

[19] R. Du Reus and F. W. Saris, *The crystallization temperature of amorphous transition-metal alloys*, Materials Lett. 9 (1990), p.p. 487 – 493.

[20] R. Bormann, F. Gärtner and F. Haider, *Determination of the free energy of equilibrium and metastable phases in the Cu-Zr system*, Materials Science and Engineering, 97 (1988), p.p. 79 – 81.

[21] M. S. El-Eskandarany and A. Inoue, *Solid-state crystalline-glassy cyclic phase transformations of mechanically alloyed $Cu_{33}Zr_{67}$ powders*, Metallurgical and Materials Transactions A, 33A (2002), p.p. 135 – 143.

[22] A. V. Davydov, U. R. Kattner, D. Josell, J. E. Blendell, R. M. Waterstrat, A. J. Shapiro, and W. J. Boettinger, *Determination of the CoTi congruent melting point and thermodynamic reassessment of the Co-Ti system*, Metallurgical and Materials Transactions A, 32A (2001), p.p. 2175 – 2186.

[23] W. Sinkler, *A Laves phase-body-centered cubic structural relationship determined using high voltage electron microscopy*, Acta mater. 40(1996), p.p.1623-1636.

[24] M.-C. Marinica, F. Willaime, and J.-P Crocombette, *Irradiation-induced formation of nanocrystallites with C15 Laves phase structure in bcc iron*, Phys. Rev. Lett. 108(2012), 025501-1~5.

Figure captions

Figure 1

Electron-irradiation-induced phase change in $E9_3$-$CoTi_2$ at 140 K at dose rate of 6.7×10^{24} m^{-2} s^{-1}, studied using in situ HVEM. Electron energy was 2 MeV. Parts (a) to (f) show sequential BF images of a fixed area, (a') to (f') show the corresponding SAED patterns, and (e") and (f") are magnified BF images corresponding to (e) and (f), respectively.

Figure 2

Electron-irradiation-induced phase change in $E9_3$-$CoTi_2$ at 220 K at dose rate of 6.7×10^{24} m^{-2} s^{-1}, studied using in situ HVEM. Electron energy was 2 MeV. Parts (a) to (f) show sequential BF images of a fixed area, (a') to (f') show the corresponding SAED patterns, and (d"), (e"), and (f") are magnified BF images corresponding to (d), (e), and (f), respectively.

Figure 3

Electron-irradiation-induced phase change in $E9_3$-$CoTi_2$ at dose rate of 7.3×10^{24} m^{-2} s^{-1}, studied using in situ HVEM. Electron energy was 2 MeV. Parts (a) and (b) show BF images of fixed area before and after irradiation for 300 s at 103 K, respectively. Parts (a') and (b') show the corresponding SAED patterns. Parts (c) to (f) show sequential BF images of the same area irradiated at 290 K for various periods, and (c') to (f') are the corresponding SAED patterns. Parts (d"), (e"), and (f") are magnified BF images corresponding to (d), (e), and (f), respectively.

Figure 4

STEM analyses of crystallites formed in amorphous phase by irradiation for 3.6×10^3 s at 290 K at dose rate of 7.3×10^{24} m^{-2} s^{-1}. Part (a) shows a BF-STEM image of crystallites (the specimen is the same as that in Figure 3f"). Part (b) is an enlarged image of area marked by a square in (a), and (c) shows the corresponding FFT pattern.

Figure 5

Temperature dependence of dose (dpa) required for amorphisation (○) and for crystallite formation (■) under 2 MeV electron irradiation. The definitions of ○ and ■ are given in the text. Note that the required dose (■) at 290 K was measured from the beginning of irradiation at 290 K, while all other doses were total doses. Dotted and broken lines are guides for the eye.

Table 1. Electron-irradiation-induced crystallisation (or partial crystallisation) of amorphous phase produced beforehand by electron irradiation.

Intnermetallic compound	Does (dpa) required to cause electron-irradiation-induced crystallisation of an amorphous phase produced beforehand by electron irradiation (temperature)	Crystal formed	Presence(○) or absence (×) of a retained amorphous phase after crystallisation	Reference	Category I or II	Information on G^{ss}-G^{am} from [literature]
Cr_2Ti	2.0 (22 K)	bcc s.s.[a)]	×	[17]	I	~ –6 kJ/mol
	2.6 (103 K)	bcc s.s.	×	[6]		[6]
Co_2Ti	80 (103 K)	hcp s.s.	○	present work	II	~ –1.7 kJ/mol
	53 (140 K)	hcp s.s.	○			[present work]
	27 (220 K)	hcp s.s.	○			
Zr_2Cu	120 (298 K) [at least, a few ten dpa]	fcc s.s.[b)]	○	[18]	II	~ +2.5 kJ/mol [14]
						negative but small [21]
Zr_2Pd	214 (103 K) [at least, a few ten dpa]	fcc s.s.[b)]	○	[9]	II	none

Electron energy was 2 MeV in all cases. a) s.s. stands for solid solution, b) after reference [16].

Figures

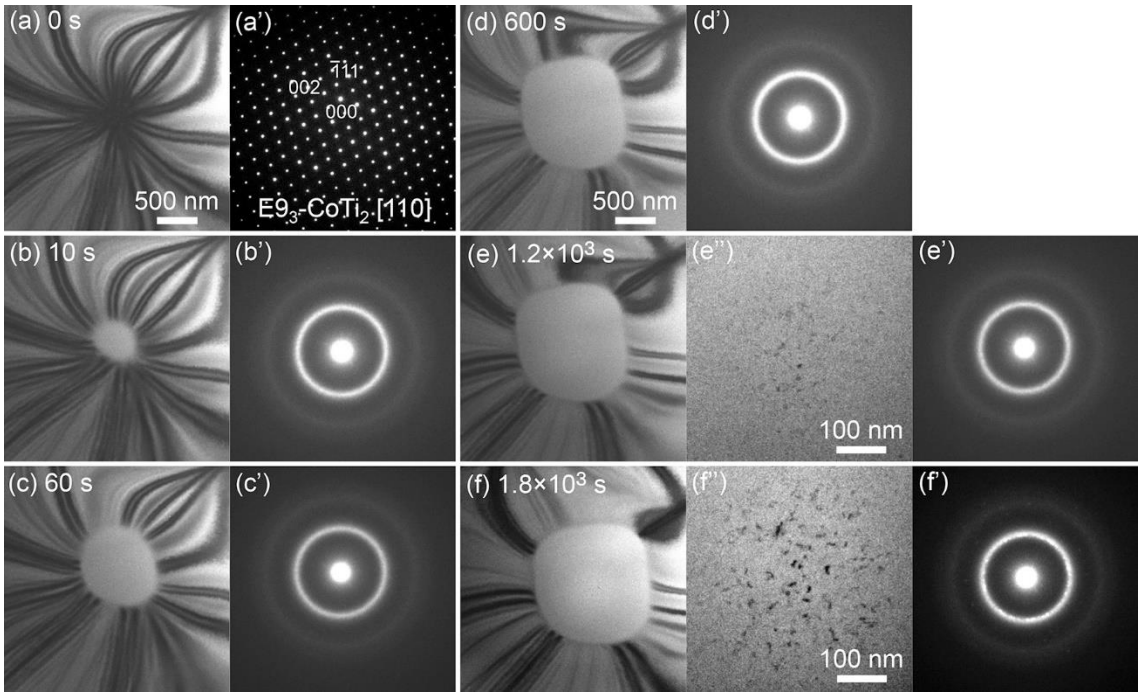

FIG.1

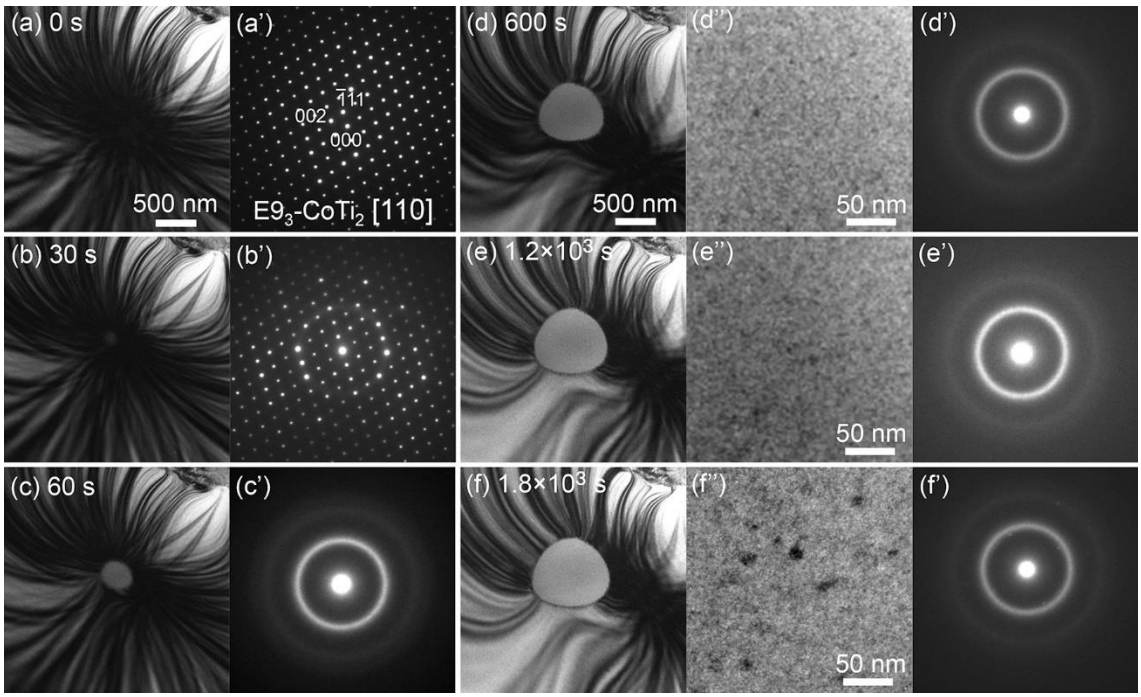
(a) 0 s
(a')
(d) 600 s
(d'')
(d')
500 nm
002
$\bar{1}1.1$
000
E9$_3$-CoTi$_2$ [110]
500 nm
50 nm
(b) 30 s
(b')
(e) 1.2×10^3 s
(e'')
(e')
50 nm
(c) 60 s
(c')
(f) 1.8×10^3 s
(f'')
(f')
50 nm

FIG.2

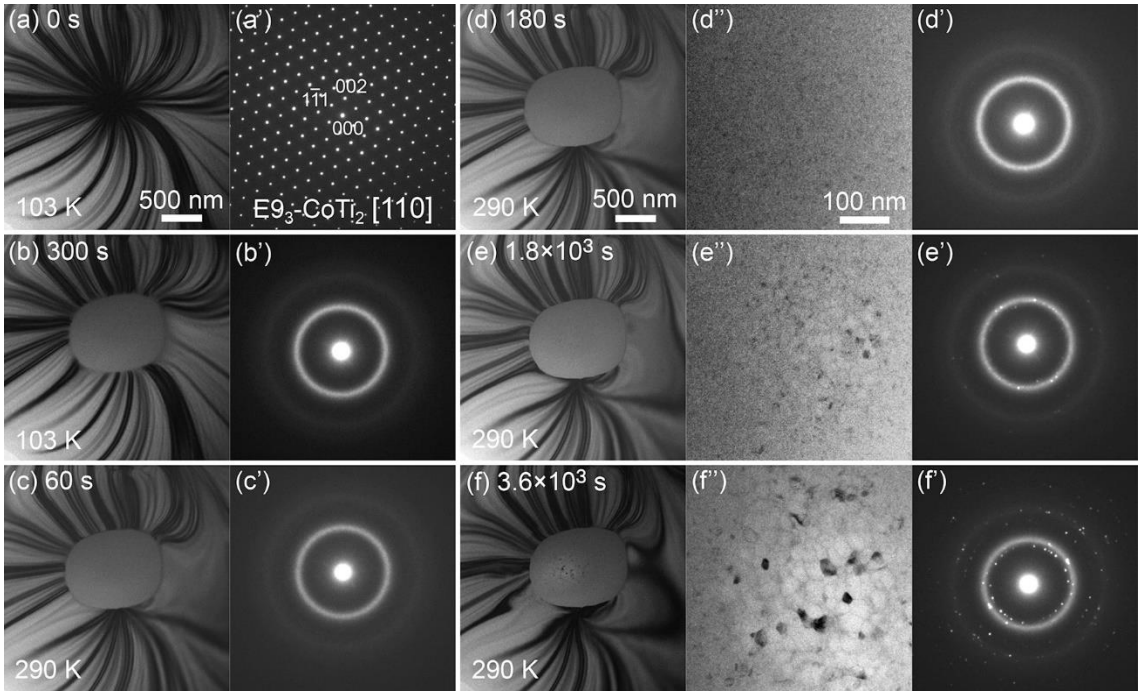
(a) 0 s
(a')
$\bar{1}11$
002
000
103 K
500 nm
E9$_3$-CoTi$_2$ [110]
(d) 180 s
(d'')
(d')
290 K
500 nm
100 nm
(b) 300 s
(b')
(e) 1.8×10^3 s
(e'')
(e')
103 K
290 K
(c) 60 s
(c')
(f) 3.6×10^3 s
(f'')
(f')
290 K
290 K

FIG.3

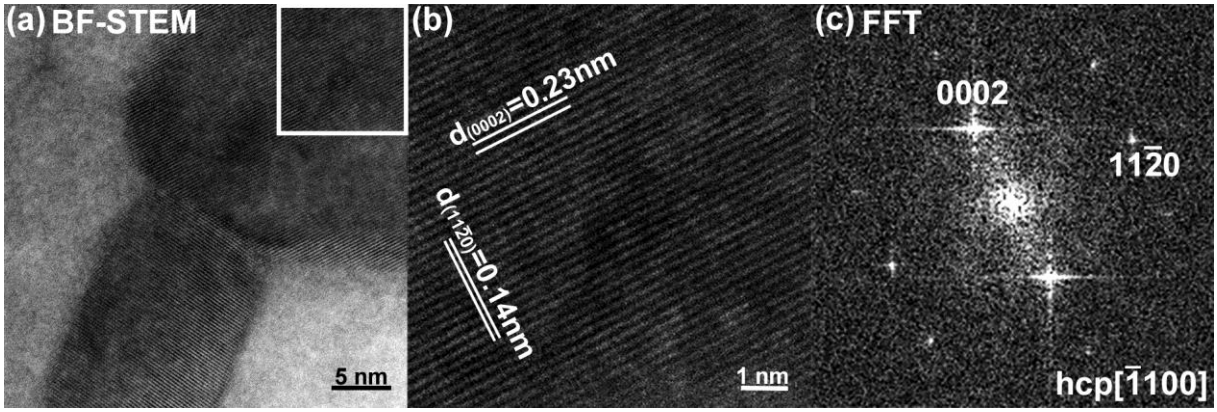
(a) BF-STEM
5 nm
(b)
d(0002)=0.23nm
d(11$\bar{2}$0)=0.14nm
1 nm
(c) FFT
0002
11$\bar{2}$0
hcp[$\bar{1}$100]

FIG.4

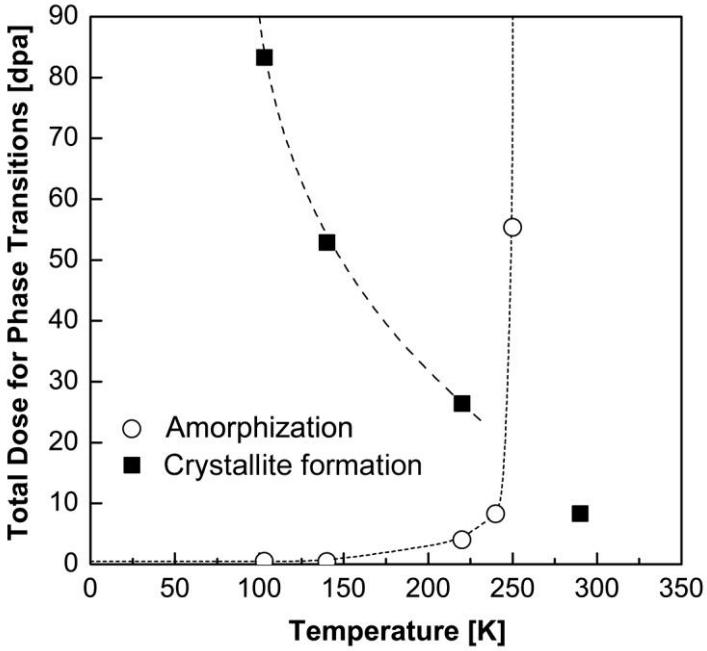
Total Dose for Phase Transitions [dpa]
Temperature [K]
Amorphization
Crystallite formation
0
10
20
30
40
50
60
70
80
90
0
50
100
150
200
250
300
350

FIG.5